Applied Catalysis B: Environmental 174–175 (2015) 43–48

Contents lists available at ScienceDirect

Applied Catalysis B: Environmental

journal homepage: www.elsevier.com/locate/apcatb

Dopamine-assisted one-step fabrication of Ag@AgCl nanophotocatalyst with tunable morphology, composition and improved photocatalytic performance

Wei Li[a,1], Zhiyuan Ma[a,b,1], Guoqiang Bai[a], Jiamei Hu[a], Xuhong Guo[a,c], Bin Dai[a,*], Xin Jia[a,*]

[a] School of Chemistry and Chemical Engineering/Key Laboratory for Green Processing of Chemical Engineering of Xinjiang Bingtuan, Key Laboratory of Materials-Oriented Chemical Engineering of Xinjiang Uygur Autonomous Region, Engineering Research Center of Materials-Oriented Chemical Engineering of Xinjiang Bintuan, Shihezi University, Shihezi 832003, People's Republic of China
[b] Département de chimie Université de Montréal C.P. 6128, Succursale Centre-Ville Montréal, Québec H3C 3J7, Canada
[c] State Key Laboratory of Chemical Engineering, East China University of Science and Technology, Shanghai 200237, People's Republic of China

ARTICLE INFO

Article history:
Received 11 December 2014
Received in revised form 15 February 2015
Accepted 21 February 2015
Available online 26 February 2015

Keywords:
Photochemistry
Plasmon photocatalysis
Self-stability
Silver
Dopamine chemistry

ABSTRACT

A green, energy-effective mussel-inspired synthetic approach for the production of a Ag@AgCl photocatalyst mediated by the polymerization of dopamine through a one-pot method at room temperature is reported. The composites with tunable morphology and compositions via the controlling the initial pH value of polymerization and concentration of PVP exhibit controlled catalytic performance under visible light. The products formed in weak alkaline perform the highest activity, good stability and recyclability, due to the suitable proportion between Ag and AgCl.

1. Introduction

Semiconductor photocatalysis has attracted considerable attention as a promising candidate for the removal of hazardous organic contaminants from air or wastewater and a green technique to produce hydrogen by water splitting [1,2] and convert carbon dioxide into gaseous hydrocarbons [3,4]. Recently, the development of a highly efficient visible light photo-catalyst has been recognized as an urgent goal in the field of photocatalysis. Two major strategies are frequently employed to produce visible light photocatalysts. One of these strategies is to modify TiO_2, a widely studied photocatalyst, via many methods such as doping [5], sensitizing [6] and coupling [7,8]. However, the limited amount and the leaching of dopants may cause poor photocatalytic efficiency. Another option is to fabricate novel visible light photocatalysts, such as Bi_2WO_6 [9], $CaFe_2O_4$/TaON [10], Ag_3AsO_4 [11], or $Cu_2(OH)PO_4$ [12]. Despite impressive progress, these photocatalysts still have some drawbacks, such as relatively low photocatalytic activity and poor stability [13]. Fabricating efficient photo-catalysts with good activity, stability and recyclability that are sensitive to visible light is still a considerable challenge.

Nanoparticles (NPs) of noble metals can absorb visible light due to the plasmon resonance of these materials, which is mainly influenced by the size and morphology [14–16]. To date, various systems that enhance plasmon resonance have been developed plasmon resonant for semiconductors based on noble metal [17], such as Ag/TiO_2/graphene [18], Pd/TiO_2 [19], Au/TiO_2 [20,21] and Ag@AgCl [22–26]. Among these systems, Ag@AgCl has attracted extensive interest, because it is a promising candidate that can meet the requirements of efficiency and stability [27,28], has high photocatalytic activity resulting from the surface plasmon resonance (SPR) of Ag nanoparticles (AgNPs) and represents a promising class of visible-light photocatalysts [29–31]. Generally, a two-step process has been used to produce such photocatalysts. The AgCl

* Corresponding authors. Present addresses: School of Chemistry and Chemical Engineering/Key Laboratory for Green Processing of Chemical Engineering of Xinjiang Bingtuan, Shihezi University, Shihezi 832003, People's Republic of China. Tel.: +86 993 2057277; fax: +86 993 2057270.
E-mail addresses: db_tea@shzu.edu.cn (B. Dai), jiaxin@shzu.edu.cn (X. Jia).
[1] These authors contribute equally to this work.

http://dx.doi.org/10.1016/j.apcatb.2015.02.029
0926-3373/

core is formed first and then the silver is reduced from Ag^+ to Ag^0. Two reduction approaches are usually employed to fabricate these catalysts, ultraviolet reduction and polyols reduction at high temperatures. As is well known, this multiple-step approach is tedious and time-consuming. Therefore, the development of a method that is both low temperature and green is still urgent in this field. Moreover, tuning the composition of Ag and AgCl, which plays a key role in the photocatalytic property, has been barely reported, because controlling the degree of reduction is difficult. It is highly desirable to develop a more facile method for controlling the composition of this material with excellent catalytic activity and stability under mild reaction conditions.

Dopamine (DA), an electrochemically active neurotransmitter, plays a significant physical role in the mammalian central nervous system. DA contains catechol and amine functional groups that can undergo spontaneously self-polymerization to deposit a polydopamine (Pdop) coating on many materials without a surface pretreatment [32–34]. More important, the nitrogen-containing groups present on the surface have metal-binding ability to absorb metal precursor onto the substrate, and the redox-active catechol group can undergo oxidation to quinone and serve as a reducing agent to reduce the metal precursor to NPs. The pH-induced reducibility of Pdop has been utilized to reduce the metal ions into metal nanoparticles [35–37]. In previous work, the polymerization rate of dopamine can be used to produce nanocatalysts with tailored size and morphology. Because DA is sensitive to oxidation, dopamine hydrochloride, a dopamine precursor, is widely used as a commercial chemical, which inspired us to use chloride ions to produce AgCl and dopamine polymerization to reduce Ag^+ and fabricate the AgNPs or Ag nanoshell. Therefore, controllable Ag@AgCl photocatalyst composites can be prepared in one-step without high temperature. Furthermore, some recent reports demonstrated that Pdop exhibited semiconducting properties and special charge transfer capabilities [38,39]. To the best of our knowledge, polydopamine has not been used as both the reactant precursor and reductant to prepare a high activity Ag@AgCl catalyst. A polydopamine-supported Ag@AgCl (P-Ag@AgCl) photocatalyst may exhibit high photosensitivity and stability under light illumination.

Herein, a polydopamine-supported Ag@AgCl (P-Ag@AgCl) photocatalyst has been prepared using dopamine hydrochloride as the reactant and reductant. Taking advantage of this new biomolecule, the compositions and properties of the as-prepared photocatalyst could be easily controlled by the values of pH and dispersant concentration, which are essential for the design and optimization of these photocatalysts. The amount of the Ag in the P-Ag@AgCl depended on the polymerization of dopamine, which influenced the photocatalytic activity. Interestingly, the composites with tunable compositions exhibited outstanding photocatalysis performance for the degradation of rhodamine B (RhB) under visible light irradiation.

2. Results and discussion

In a typical experiment, dopamine hydrochloride (0.18 g) and poly(vinylpyrrolidone) (PVP) (0.27 g) were dissolved in 55 mL of deionized water, and the pH of the mixed was adjusted using 1 M NaOH and 1 M HCl. Subsequently, an aqueous solution $AgNO_3$ (3.5 wt%) was injected into the solution to give a final volume of 60 mL and then vigorously stirred for 30 min. The mole rate of dopamine hydrochloride is higher than that of Ag^+ so that the chloride source is sufficient. During this process, the precipitation reaction between Ag^+ ions and Cl^- ions and preparation of AgNPs were occurred at the same time. The synthesis parameters, such as the initial pH value of the solution and PVP concentration, play a crucial role in the synthesis. Herein, we select the influence of the pH value and the amount of PVP on controlling the composition and morphology of P-Ag@AgCl.

The surfactant PVP is popular in many syntheses. While many molecules can interfere with the growth of nanocrystals, the molecules promote nanoparticle aggregation. Thus, the "decentralizing" issue must be addressed. PVP remains the optimal choice

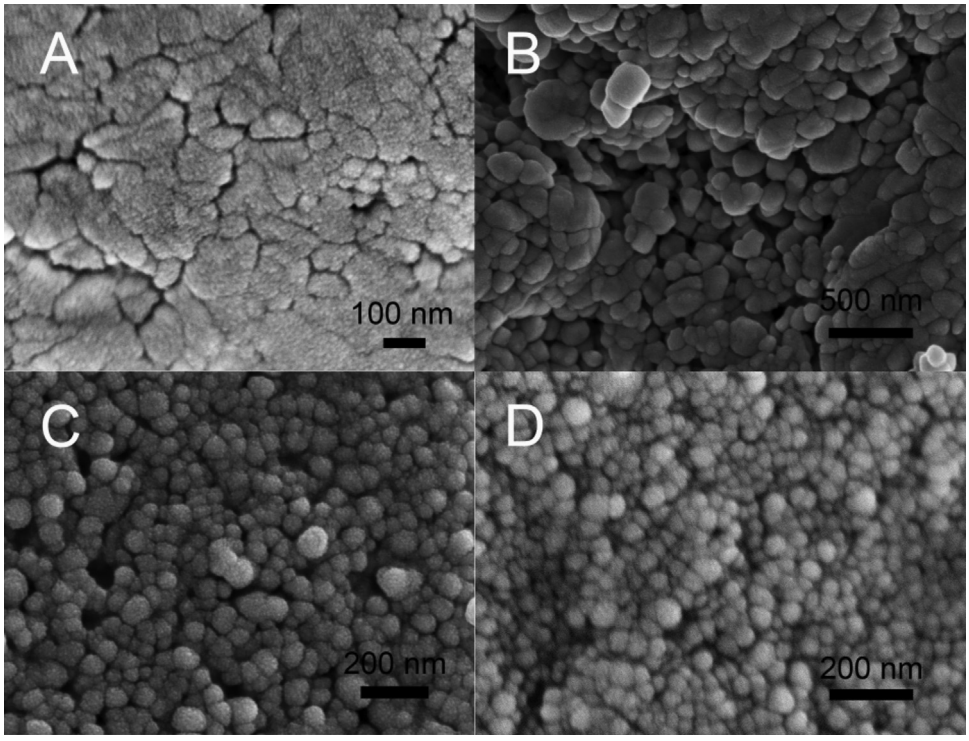

Fig. 1. Typical FESEM images of (A) P-Ag@AgCl–PVP-0, (B) P-Ag@AgCl–PVP-2, (C) P-Ag@AgCl–PVP-4.5, (D) P-Ag@AgCl–PVP-9.0.

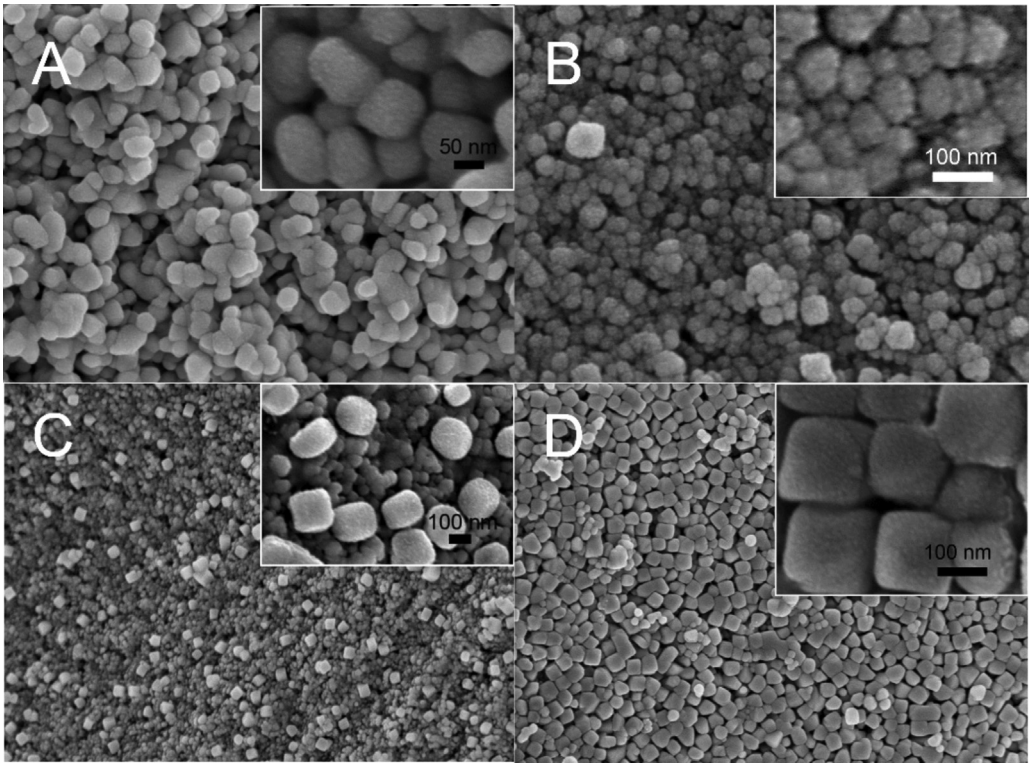

Fig. 2. Typical FESEM images of (A) P-Ag@AgCl–pH-2.1, (B) P-Ag@AgCl–pH-7.8, (C) P-Ag@AgCl–pH-9.0, and (D) P-Ag@AgCl–pH-11.0.

for a balanced solution for this problem. First, we present a study of the roles of PVP in the synthesis of P-Ag@AgCl. Fig. 1(A–D) shows the effect of PVP on the morphology of the products synthesized at PVP concentrations of 0 mg/mL, 2 mg/mL, 4.5 mg/mL and 9.0 mg/mL, and these products are noted as P-Ag@AgCl–PVP-0 to 9.0. As Fig. 1A reveals, P-Ag@AgCl–PVP-0 was prepared without PVP and is similar to the bulk material, although some parts have different diameters. For P–Ag@AgCl–PVP–2.0, some aggregated nanoparticles appear. Plenty of monodisperse photocatalysts with smaller sizes are formed at higher concentrations of PVP; for example, P–Ag@AgCl–PVP–4.5 and P–Ag@AgCl–PVP–9.0 have products with diameters of approximately 78 nm and 40 nm, respectively.

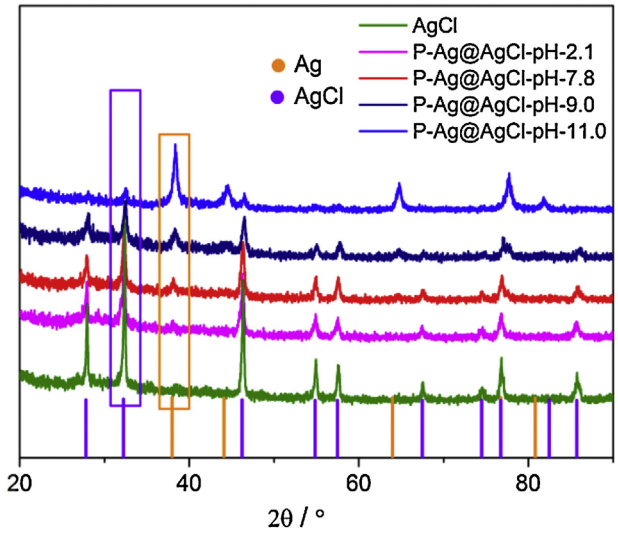

Fig. 3. XRD patterns of P-Ag@AgCl in different pH value.

Considering that PVP can hinder Pdop formation, we selected 4.5 mg/mL PVP as the optimum.

The pH is another important factor for P-Ag@AgCl. Different initial pH values were used to fabricate P-Ag@AgCl. Fig. 2 presents field emission scanning electron microscopy (FESEM) images of the P-Ag@AgCl. As soon as the $AgNO_3$ solution was added to dopamine solutions with different pH values, the mixed solution turned into different colors (Fig. S1). The color of the dispersed particles deepens as the solution pH increases. Fig. 1(A–D) shows the P-Ag@AgCl synthesized at pH value of 2.1, 7.8, 9.0 and 11.0, and the products are noted as P–Ag@AgCl–PVP–2.1 to 11.0. Interestingly, these nanoparticles exhibit clearly different shapes and compositions with the pH value increasing. P-Ag@AgCl spheres with diameters of approximately 100 nm and 80 nm can be found in Fig. 2A (pH 2.1) and B (pH 7.8), respectively. Whereas some of the photocatalysts exhibit an ideal sphere-like shape, other P-Ag@AgCl composites show shape-deformation. When the pH value increases to an alkaline value (pH 9.0), silver cubic cages are mixed in the product, as shown in Fig. 2C. Compared with photocatalysts produced in acidic and weak alkaline reaction environment, P-Ag@AgCl formed at pH 11.0 are mostly nanoparticles that exhibit cubic morphologies and uniform sizes with an average edge length of 200 nm. Elemental analysis of the Ag:AgCl hybrid nanoparticles is carried out with energy dispersive X-ray spectroscopy (EDS) (Supporting information, Fig. S2). The results show the rate of Ag to AgCl and the amount of nitrogen and carbon in the products increase with the increase in pH value. This phenomenon may be attributed to the reducing capacity and the polymerization rate of dopamine in different pH solutions.

The phase structure of the resultant P-Ag@AgCl nanocompsites were analyzed by XRD, as seen in Fig. 3. The pattern can be indexed to the cubic phase of AgCl with lattice constant $a = 5.5491$ Å (JCPDS card 31-1238). For P–Ag@AgCl–PVP–2.1, it is hard to detect Ag peaks in the XRD pattern. The XRD pattern of P–Ag@AgCl–PVP–7.8 to 11.0 reveals the additional (1 1 1), (2 0 0), and (2 2 0) planes for Ag (JCPDS card 89-3722), which means Ag nanoparticles are

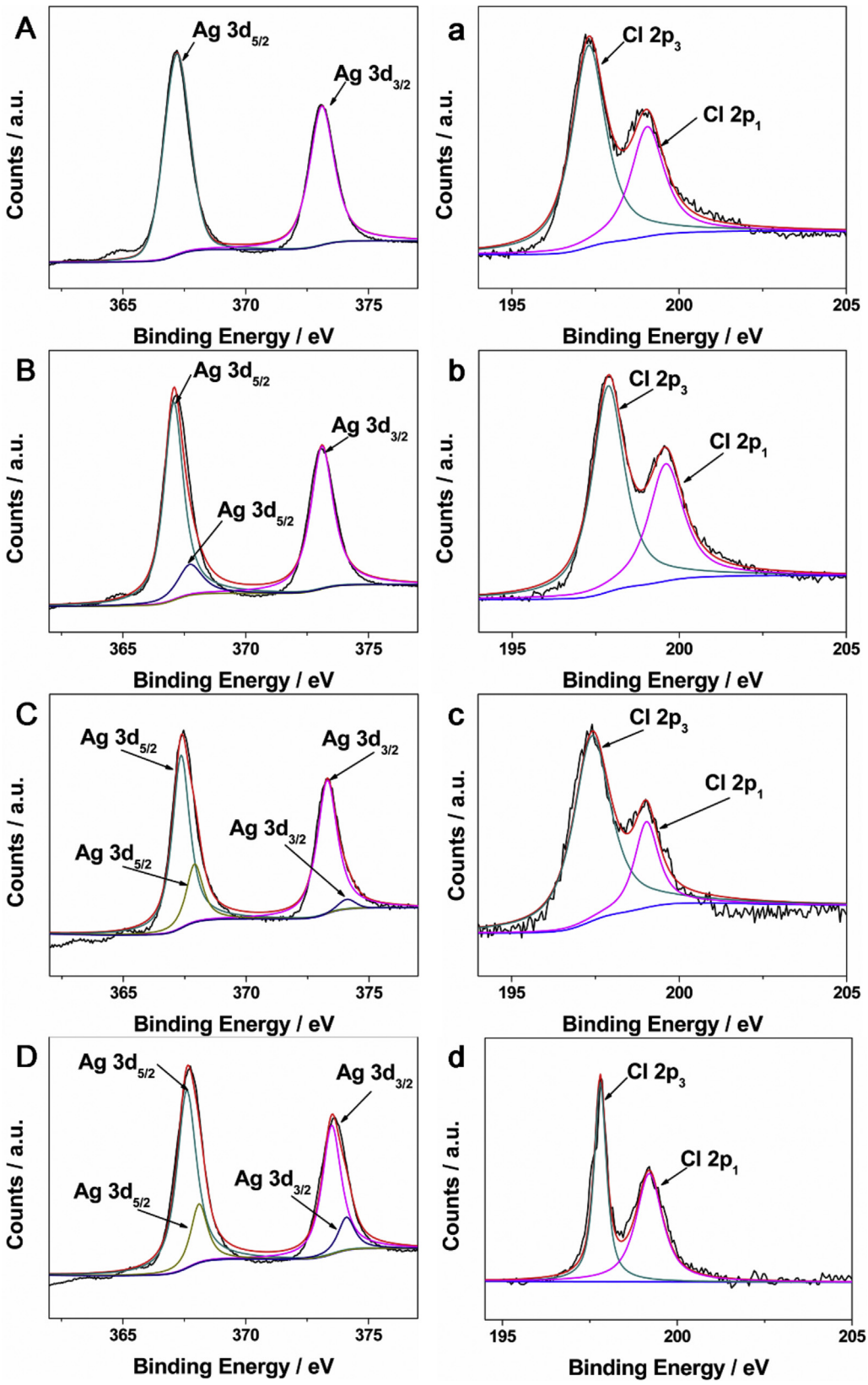

Fig. 4. XPS spectra of Ag 3d (A–D) and Cl 2p (a–d) of (A) P-Ag@AgCl–pH-2.1, (B) P-Ag@AgCl–pH-7.8, (C) P-Ag@AgCl–pH-9.0, and (D) P-Ag@AgCl–pH-11.0.

successfully produced. With the initial pH solution increase, the XRD pattern peaks of Ag sharpened and cubic morphology indicate well crystalline of silver nanoparticles.

To further confirm the Ag species on the surface of P-Ag@AgCl, the as-obtained samples were characterized by X-ray photoelectron spectroscopy (XPS). As shown in Fig. 4a–d, the Cl species display a binding energies of Cl $2p_3$ and Cl $2p_1$ at about 197.3 and 199.1 eV, respectively. Besides, two bands at ca. 367.2 and 373.2 eV, which could be ascribed to Ag $3d_{5/2}$ and Ag $3d_{3/2}$ binding energies, respectively, could also be observed (Fig. 4A and

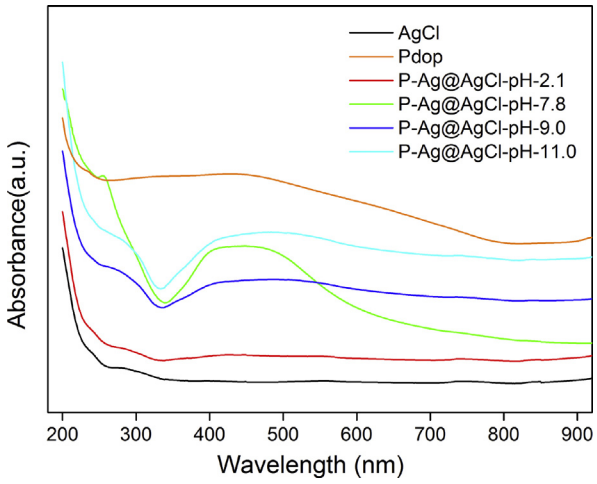

Fig. 5. Absorption spectra of the P-Ag@AgCl nanoparticles.

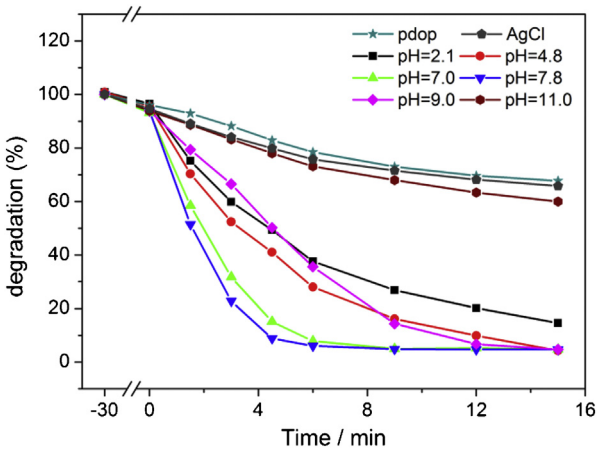

Fig. 6. Photocatalytic degradation of RhB (50 mL, 5 mg/mL) over different photocatalysts (5 mg) under visible light irradiation ($\lambda > 420$ nm).

B). Usually, these two bands could be further deconvoluted into two sets of peaks at 367.4, 368.0 eV, and 373.3, 374.1 eV, respectively. Those at 367.4 and 373.3 eV could be assigned to the Ag^+ species of AgCl, while those at 368.0 and 374.1 eV could be attributed to the metallic Ag^0 species [40]. However, because of different reaction conditions, the two bands of different samples were deconvoluted into different peaks. The semiquantitatively calculated mole ratio between Ag^0 and Ag^+ in P–Ag@AgCl–PVP–2.1 to 11.0 is 0, 0.11, 0.19 and 0.26, respectively. These results confirm the compositions in the composites, further indicating the formation of the P-Ag@AgCl.

Strong coupling of the SPR effect of AgNPs or the SPR effect of Ag nanoshells is responsible for the strong absorption of the P-Ag@AgCl hybrid nanoparticles in the visible light region (Fig. 5). The AgCl dispersion looks milky in color and exhibits strong absorption only in the ultraviolet spectral region. Dispersed Pdop displays a black color, which materializes in monotonic absorption at wavelengths approximately 500 nm. The absorption spectra of P-Ag@AgCl formed at different pH values show different absorption performance in the visible region. For an acidic solution (pH 2.1), the absorption of P–Ag@AgCl–PVP–2.1 is almost same as AgCl and absorbs only in the ultraviolet region. For an alkaline environment, the product shows strong absorption in the visible spectral region, which is attributed to the SPR effect of AgNPs in AgCl or on the surfaces of AgCl. In contrast, a higher initial pH promotes the formation of Pdop, so the absorption between 300 and 800 nm decreases, which indicates progressive formation of polydopamine.

Photocatalytic performance of the P-Ag@AgCl hybrid nanoparticles has been evaluated by degradation of dye molecules, i.e., rhodamine B (RhB), under the visible light illumination. The bulk forms of AgCl and polydopamine were used for comparison. In a typical experiment of RhB photodegradation, 5 mg of the samples was added to 50 mL RhB aqueous solution (5 mg L^{-1}) at room temperature. Prior to irradiation, the mixture of the catalyst and RhB solution was stirred for 30 min in the dark to obtain an adsorption–desorption equilibrium. The concentration of the dye solution decreases slightly in the dark because of the adsorption, so that the C/C_0 value is slightly smaller than 100% at $t = 0$. As the irradiation time goes on, the decomposition of RhB dye progresses steadily, and different catalysts show different photoactivities. As shown in Fig. 6, both bulk AgCl and polydopamine can only decompose about 30% of RhB within 15 min of visible light irradiation while P-Ag@AgCl shows superior photocatalytic activity. For P–Ag@AgCl–PVP–2.1, they can nearly decompose 90% of dye molecules, and the decomposition of RhB over P–Ag@AgCl–PVP–4.8 is completed in 15 min of visible-light irradiation. Possibly there were low content and high dispersity of AgNPs in the photocatalysts during reaction process. When the reaction undergo in neutral and weak basic, the product of the degradation of RhB is greater than that in acid. Both P–Ag@AgCl–PVP–7.0 and P–Ag@AgCl–PVP–7.8 completely decompose 5 mg L^{-1} RhB within 6 min, and the later shows a higher activity. When the pH increases to 9.0 and 11.0, the photoactivity of precipitate decreases noticeably during the same interval, and P–Ag@AgCl–PVP–11.0 can only decompose around 40% of RhB. This may be due to the product have a higher proportion of AgNPs which could improve photoactivity with the SPR absorption, but Ag cannot degrade dye by itself. It is clearly noted that at pH values below the 7.8, degradation increased as pH increased, but above the 7.8 decreased as pH increased. The different degradation activity between produce is corroding to the rate between Ag and AgCl. To minimize the dye self-photosensitization process, phenol, which has no absorption in the visible region, was chosen as a model pollutant to evaluate the photocatalytic process of the as-prepared photocatalyst under visible light irradiation (Fig. S3). Among these samples, P–Ag@AgCl–PVP–7.8 exhibits the best photocatalytic activity.

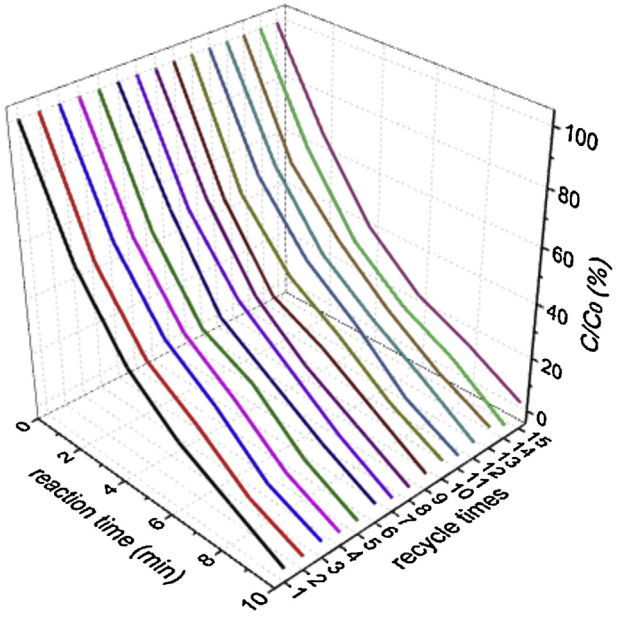

Fig. 7. Degradation kinetics of RhB molecules for 15 successive reactions catalyzed with the nanoparticles under visible-light irradiation.

In addition to efficiency, stability and recyclability of photocatalysts are also important for applications. The photocatalysts sometimes suffer from instability under repeated use owing to photo-corrosion in practical applications [41–43]. P-Ag@AgCl–pH-7.8 was selected as a model photocatalyst to test the repeatability of RhB bleaching, and we carried out the bleaching experiment 15 times. Fig. 7 plots the kinetic curves for degradation of dye solutions using the same photocatalyst. The RhB dye is quickly bleached after every injection of the RhB solution, and the catalytic efficiency of the hybrid nanoparticles does not significantly decrease even after 15 reactions.

As we know, DA cannot polymerize to form Pdop when using oxygen as the oxidant under acidic conditions and Pdop can reduce Ag^+ ions under basic environments [44]. At pH 2.1, DA is difficult to polymerize and Ag^+ can hardly be reduced. Therefore, the active composition in the obtained P–Ag@AgCl–PVP–2.1 is actually AgCl. At pH 7.8, DA polymerizes and the Ag^+ is reduced to Ag. The active compositions in P–Ag@AgCl–PVP–7.8 are AgCl and Ag. At pH 9.0 and pH 11.0, DA polymerizes more quickly and more Ag^+ ions are reduced to Ag. Although the large band gaps of AgCl cause the difficulty for exciting AgCl nanoparticles with visible light, incorporating Ag nanostructures with strong visible SPR with AgCl catalysts can increase their absorption efficiency in the visible region [23]. In addition, Ag can accelerate the separation of photogenerated holes and electrons [24]. However, when the amount of silver is large to some extent, Ag can serve as the combination center of photogenerated carriers. Pdop can also have special charge transfer abilities [38,45]. Therefore, the pH influences the polymerization of DA and DA polymerization depend on the formation of Ag^0. In this way, the compositions and properties of the as-prepared photocatalyst could be easily controlled by the values of pH. The above discussions can also be used to explain why P–Ag@AgCl–PVP–7.8 has the best photocatalytic performance.

3. Conclusions

In this work, a green, energy-effective mussel-inspired technology was developed for the production of an effective Ag@AgCl photocatalyst through a one-pot approach at room temperature. The novel photocatalyst with tunable morphology and compositions show superior photocatalytic performance in the degradation of RhB and phenol. The morphologies and compositions of P-Ag@AgCl could be tuned by controlling the initial pH value and concentration of PVP. The as-synthesized hybrid nanoparticles exhibit high efficiency for catalyzing the decomposition of the RhB dye under visible light illumination as well as high stability and recyclability. The enhanced photocatalytic efficiency in the visible spectral region is enabled by the strong SPR of the AgNPs in the hybrid nanoparticles. This control over the morphologies and compositions of photocatalysts are of great importance in practical applications.

Acknowledgment

This work was supported by the Natural Science Foundation of China (21264013, 21364010) and the Technology Foundation for Selected Overseas Chinese Scholar, Ministry of Human Resources and Social Security of the People's Republic of China.

Appendix A. Supplementary data

Supplementary data associated with this article can be found, in the online version, at http://dx.doi.org/10.1016/j.apcatb.2015.02.029.

References

[1] X. Chen, S. Shen, L. Guo, S.S. Mao, Chem. Rev. 110 (2010) 6503–6570.
[2] S.U. Khan, M. Al-Shahry, W.B. Ingler, Science 297 (2002) 2243–2245.
[3] M. Cokoja, C. Bruckmeier, B. Rieger, W.A. Herrmann, F.E. Kuhn, Angew. Chem. Int. Ed. 50 (2011) 8510–8537.
[4] S.C. Roy, O.K. Varghese, M. Paulose, C.A. Grimes, ACS Nano 4 (2010) 1259–1278.
[5] S. Livraghi, S. Maurelli, M.C. Paganini, M. Chiesa, E. Giamello, Angew. Chem. Int. Ed. 50 (2011) 8038–8040.
[6] H. Pang, H. Yang, C.X. Guo, J. Lu, C.M. Li, Chem. Commun. (Camb.) 48 (2012) 8832–8834.
[7] Z. Hu, Y. Huang, S. Sun, W. Guan, Y. Yao, P. Tang, C. Li, Carbon 50 (2012) 994–1004.
[8] B.K. Vijayan, N.M. Dimitrijevic, D. Finkelstein-Shapiro, J. Wu, K.A. Gray, ACS Catal. 2 (2012) 223–229.
[9] J. Tian, Y.H. Sang, G.W. Yu, H.D. Jiang, X.N. Mu, H. Liu, Adv. Mater. 25 (2013) 5075–5080.
[10] E.S. Kim, N. Nishimura, G. Magesh, J.Y. Kim, J.W. Jang, H. Jun, J. Kubota, K. Domen, J.S. Lee, J. Am. Chem. Soc. 135 (2013) 5375–5383.
[11] J.T. Tang, Y.H. Liu, H.Z. Li, Z. Tan, D.T. Li, Chem. Commun. 49 (2013) 5498–5500.
[12] G. Wang, B.B. Huang, X.C. Ma, Z.Y. Wang, X.Y. Qin, X.Y. Zhang, Y. Dai, M.H. Whangbo, Angew. Chem. Int. Ed. 52 (2013) 4810–4813.
[13] H. Shi, J. Chen, G. Li, X. Nie, H. Zhao, P.-K. Wong, T. An, ACS Appl. Mater. Interfaces 5 (2013) 6959–6967.
[14] Y.N. Xia, Y.J. Xiong, B. Lim, S.E. Skrabalak, Angew. Chem. Int. Ed. 48 (2009) 60–103.
[15] P.K. Jain, X.H. Huang, I.H. El-Sayed, M.A. El-Sayed, Acc. Chem. Res. 41 (2008) 1578–1586.
[16] J. Homola, Chem. Rev. 108 (2008) 462–493.
[17] W. Hou, S.B. Cronin, Adv. Funct. Mater. 23 (2013) 1612–1619.
[18] Y. Wen, H. Ding, Y. Shan, Nanoscale 3 (2011) 4411–4417.
[19] Q. Ye, X. Wang, H. Hu, D. Wang, S. Li, F. Zhou, J. Phys. Chem. C 113 (2009) 7677–7683.
[20] Y.S. Chen, H. Choi, P.V. Kamat, J. Am. Chem. Soc. 135 (2013) 8822–8825.
[21] J. Lu, P. Zhang, A. Li, F. Su, T. Wang, Y. Liu, J. Gong, Chem. Commun. (Camb.) 49 (2013) 5817–5819.
[22] Y. Tang, Z. Jiang, G. Xing, A. Li, P.D. Kanhere, Y. Zhang, T.C. Sum, S. Li, X. Chen, Z. Dong, Z. Chen, Adv. Funct. Mater. 23 (2013) 2932–2940.
[23] C. An, S. Peng, Y. Sun, Adv. Mater. 22 (2010) 2570–2574.
[24] B. Ma, J. Guo, W.-L. Dai, K. Fan, Appl. Catal. B Environ. 130–131 (2013) 257–263.
[25] L. Han, P. Wang, C. Zhu, Y. Zhai, S. Dong, Nanoscale 3 (2011) 2931–2935.
[26] Y. Xu, H. Xu, H. Li, J. Yan, J. Xia, S. Yin, Q. Zhang, Colloids Surf. A 416 (2013) 80–85.
[27] C. An, R. Wang, S. Wang, X. Zhang, J. Mater. Chem. 21 (2011) 11532–11536.
[28] C. An, X. Ming, J. Wang, S. Wang, J. Mater. Chem. 22 (2012) 5171–5176.
[29] D.L. Chen, M.N. Liu, Q.Q. Chen, L.F. Ge, B.B. Fan, H.L. Wang, H.X. Lu, D.Y. Yang, R. Zhang, Q.S. Yan, G.S. Shao, J. Sun, L. Gao, Appl. Catal. B Environ. 144 (2014) 394–407.
[30] B.W. Ma, J.F. Guo, W.L. Dai, K.N. Fan, Appl. Catal. B Environ. 130 (2013) 257–263.
[31] Y.X. Tang, V.P. Subramaniam, T.H. Lau, Y.K. Lai, D.G. Gong, P.D. Kanhere, Y.H. Cheng, Z. Chen, Z.L. Dong, Appl. Catal. B Environ. 106 (2011) 577–585.
[32] H. Lee, S.M. Dellatore, W.M. Miller, P.B. Messersmith, Science 318 (2007) 426–430.
[33] C.J. Ochs, T. Hong, G.K. Such, J. Cui, A. Postma, F. Caruso, Chem. Mater. 23 (2011) 3141–3143.
[34] B. Yu, D.A. Wang, Q. Ye, F. Zhou, W. Liu, Chem. Commun. (Camb.) (2009) 6789–6791.
[35] J. Zhou, B. Duan, Z. Fang, J. Song, C. Wang, P.B. Messersmith, H. Duan, Adv. Mater. 26 (2014) 701–705.
[36] E.K. Jeon, E. Seo, E. Lee, W. Lee, M.K. Um, B.S. Kim, Chem. Commun. (Camb.) 49 (2013) 3392–3394.
[37] X.-C. Liu, G.-C. Wang, R.-P. Liang, L. Shi, J.-D. Qiu, J. Mater. Chem. A 1 (2013) 3945–3953.
[38] H.J. Nam, J. Cha, S.H. Lee, W.J. Yoo, D.-Y. Jung, Chem. Commun. 50 (2014) 1458–1461.
[39] H.J. Nam, B. Kim, M.J. Ko, M. Jin, J.M. Kim, D.Y. Jung, Chemistry 18 (2012) 14000–14007.
[40] Y. Shen, P. Chen, D. Xiao, C. Chen, M. Zhu, T. Li, W. Ma, M. Liu, Langmuir 31 (2015) 602–610.
[41] Q. Xiang, J. Yu, B. Cheng, H. Ong, Chem. Asian J. 5 (2010) 1466.
[42] J. Yu, G. Dai, B. Huang, J. Phys. Chem. C 113 (2009) 16394–16401.
[43] J. Krýsa, K. Bouzek, C. Stollberg, J. Appl. Electrochem. 30 (2000) 1033–1041.
[44] Y. Liu, K. Ai, L. Lu, Chem. Rev. 114 (2014) 5057–5115.
[45] M. Lee, J.U. Kim, J.S. Lee, B.I. Lee, J. Shin, C.B. Park, Adv. Mater. 26 (2014) 4463–4468.